Environmental Science
Processes & Impacts

PAPER

Cite this: *Environ. Sci.: Processes Impacts*, 2014, **16**, 2711

Effect of permafrost properties on gas hydrate petroleum system in the Qilian Mountains, Qinghai, Northwest China

Pingkang Wang,*[a] Xuhui Zhang,[b] Youhai Zhu,[a] Bing Li,[c] Xia Huang,[a] Shouji Pang,[a] Shuai Zhang,[a] Cheng Lu[a] and Rui Xiao[d]

The gas hydrate petroleum system in the permafrost of the Qilian Mountains, which exists as an epigenetic hydrocarbon reservoir above a deep-seated hydrocarbon reservoir, has been dynamic since the end of the Late Pleistocene because of climate change. The permafrost limits the occurrence of gas hydrate reservoirs by changing the pressure–temperature (*P*–*T*) conditions, and it affects the migration of the underlying hydrocarbon gas because of its strong sealing ability. In this study, we reconstructed the permafrost structure of the Qilian Mountains using a combination of methods and measured methane permeability in ice-bearing sediment permafrost. A relationship between the ice saturation of permafrost and methane permeability was established, which permitted the quantitative evaluation of the sealing ability of permafrost with regard to methane migration. The test results showed that when ice saturation is >80%, methane gas can be completely sealed within the permafrost. Based on the permafrost properties and genesis of shallow gas, we suggest that a shallow "gas pool" occurred in the gas hydrate petroleum system in the Qilian Mountains. Its formation was related to a metastable gas hydrate reservoir controlled by the *P*–*T* conditions, sealing ability of the permafrost, fault system, and climatic warming. From an energy perspective, the increasing volume of the gas pool means that it will likely become a shallow gas resource available for exploitation; however, for the environment, the gas pool is an underground "time bomb" that is a potential source of greenhouse gas.

Received 10th September 2014
Accepted 20th October 2014

DOI: 10.1039/c4em00482e

rsc.li/process-impacts

Environmental impact

The gas hydrate petroleum system in the Qilian Mountains permafrost is an epigenetic hydrocarbon reservoir situated over a deep-seated hydrocarbon reservoir, which has been dynamic since the end of the Late Pleistocene because of climatic changes. The permafrost not only limits the occurrence of the gas hydrate reservoir by changing the *P*–*T* conditions, but also affects the migration of underlying hydrocarbon gas because of its strong sealing ability. This study established the relationship between permafrost ice saturation and methane permeability, which suggests that under the influence of a warming climate, a shallow gas pool has formed in the Qilian Mountains gas hydrate petroleum system, because of the *P*–*T* conditions, sealing ability of permafrost, and the fault system.

1. Introduction

Gas hydrates are crystalline solids composed solely of water and gas. Their structure comprises gas molecules ("guests") that are trapped within water cavities ("hosts") composed of hydrogen-bonded water molecules.[1] A wide variety of potential guest molecules can occur in nature, including CO_2, N_2, H_2S, and C_2H_6, although the predominant guest molecule is methane (CH_4).[2] Gas hydrates are stable under conditions of high pressure and relatively low temperature and their formation and/or decomposition depend on the pressure, temperature, composition of gas, salinity of coexisting water, and characteristics of the porous medium in which they are formed.[3] These pressure and temperature (*P*–*T*) requirements restrict the global distribution of gas hydrates to permafrost regions and marine sediments on continental margins.[4] On Earth today, permafrost covers a large proportion of high-altitude and high-latitude land in both hemispheres.[5] Gas hydrate is known to have accumulated in Arctic regions in association with the permafrost in western Siberia, Russia,[3] the Alaskan North Slope, the United States,[6] and the Mackenzie Delta, Canada.[7,8] In addition, gas hydrates have been found in the permafrost of the Qilian Mountains in the

[a]*Oil and Gas Survey, China Geological Survey, Beijing, 100029, PR China. E-mail: wangpk@cags.ac.cn; Fax: +86 10 64304688; Tel: +86 10 64697552*
[b]*Institute of Mechanics, Chinese Academy of Sciences, Beijing, 100190, PR China*
[c]*College of Construction and Engineering, Jilin University, Changchun, 130021, PR China*
[d]*Institute of Mineral Resources, Chinese Academy of Geological Sciences, Beijing, 100037, PR China*

Qinghai Province of China, which is a mid-latitude region of high elevation.[9]

The gas hydrate system in the permafrost of the Qilian Mountains is considered an epigenetic hydrocarbon reservoir situated over a deep-seated hydrocarbon reservoir.[10] This gas hydrate reservoir has a shallower depth (133–396 m), thinner permafrost (60–95 m; locally exceeding 100 m), and a more complex gas composition (54–76% CH_4, 8–15% C_2H_6, 4–21% C_3H_8, 1–7% CO_2) than the well-documented Arctic hydrate reservoir.[9,11] It was classified by Boswell *et al.*[12] and Koh *et al.*[13] as type R, because the hydrate deposits occur within various rock types, in contrast to type C reservoirs, where the hydrate deposits occur in unconsolidated coarse-grained sediments. Between 2008 and 2011, eight gas hydrate wells (DK-1 to DK-8) were drilled in the permafrost of the Muri coalfield in South Qilian. Gas hydrate samples were recovered from boreholes DK-1, DK-2, DK-3, DK-7, and DK-8, and anomalies known to be associated with the presence of hydrates were observed in boreholes DK-4, DK-5, and DK-6 (Fig. 1). While drilling through the permafrost and gas-hydrate-bearing layer, gas blowouts occurred (Fig. 2), similar to those reported when drilling gas hydrates in the Arctic permafrost. The phenomenon of abrupt and intense gas blowouts was interpreted as a consequence of the rapid decomposition of the gas hydrate due to the sudden changes in *P–T* conditions during the drilling.[7,14,15] However, the gas blowouts that occurred in the Qilian Mountains appear slightly different than those reported from the Arctic. As the depth of the gas hydrate pay zone is deeper than the permafrost by about 40 m or more in the Qilian Mountains, it appears that there is no direct link between the gas blowouts that occurred in the inner layer of the permafrost and the deeper gas hydrate. In addition, some cases of drilling for coal also encountered gas blowouts in the permafrost. Thus, some researchers speculated that the main source of gas blowouts might be shallow microbial gas. However, there are no reliable data to support this hypothesis. In 2013, two gas hydrate wells (DK-9 and DK-10) were completed in this area (Fig. 1). As expected, gas hydrate samples were recovered successfully from borehole DK-9; however, unexpectedly, borehole DK-10 encountered unprecedented strong gas blowouts at a depth of 52.9 m in the permafrost, the flame height of which rose to 3–4 m and the gas flow was >4800 m^3per day[16] Subsequently, the borehole was plugged in order to prevent further accidents. Therefore, gas blowouts not only act as potential indicators for gas hydrates, but they also can be the cause of drilling accidents. Recently, the migration of the gas hydrate stability zone (GHSZ) in the permafrost of the Qilian Mountains was confirmed by evidence from fracture-filling pyrite morphology and pyrite sulfur isotopes.[11] The migration of the GHSZ, *i.e.*, the top and bottom of the GHSZ have moved downward and upward to a certain extent, respectively, has caused the decomposition of gas hydrates, which has released methane near the top and the bottom of the GHSZ. Part of the methane was involved in anaerobic methane oxidation, bacterial sulfate reduction, and other bio-geochemical process that have contributed to episodes of mineralization of calcite, pyrite, alstonite, and

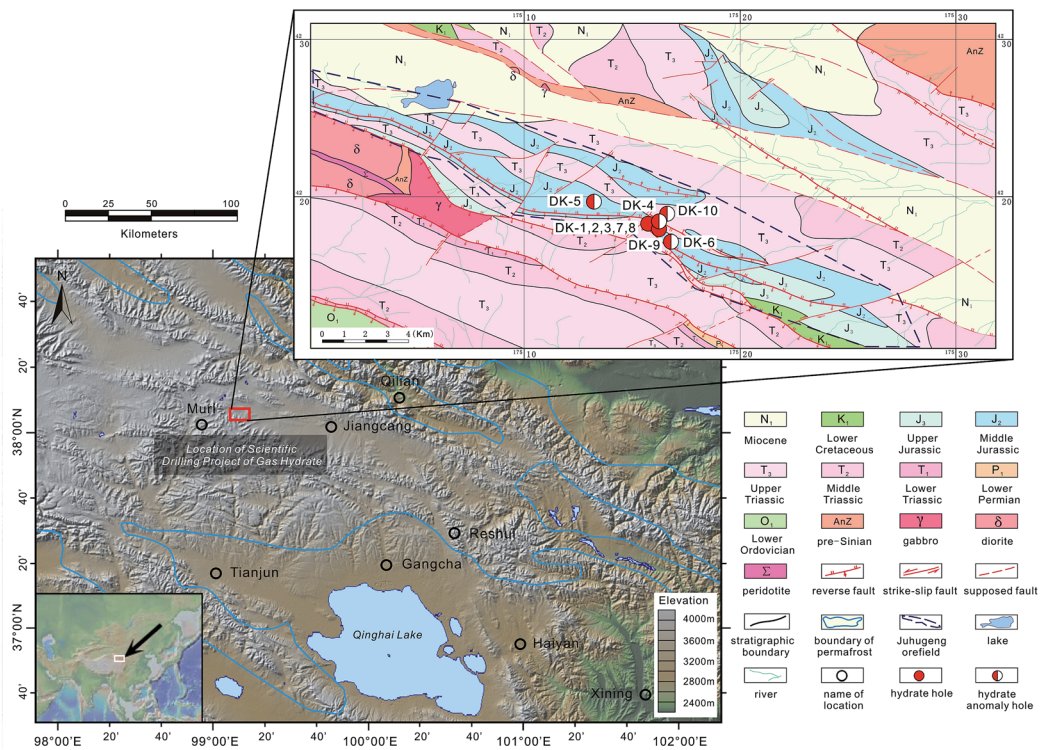

Fig. 1 Location of the Scientific Drilling Project of Gas Hydrates and the geological map for the area studied in the Qilian Mountains permafrost (geomorphology data from Ryan *et al.*[66] and permafrost distribution from Zhou *et al.*[19]).

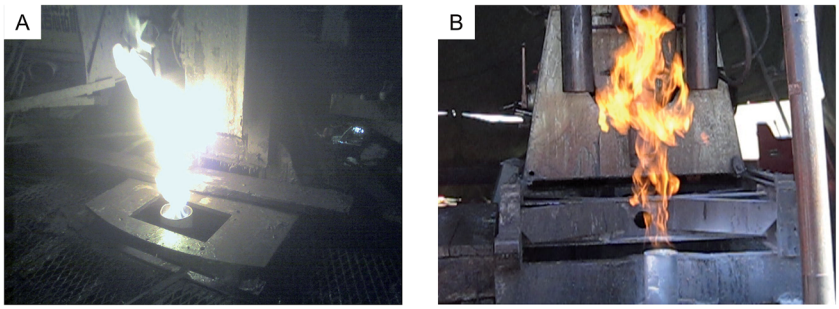

Fig. 2 Gas blowouts and burning phenomena during gas hydrate drilling in the Qilian Mountains permafrost: (A) gas blowout occurred at a depth of 105 m in the DK-4 borehole; (B) gas blowout occurred at a depth of 114 m in the DK-7 borehole.

ankerite,[10,17,18] while most of the remaining methane exists as free gas. Therefore, one question to be addressed is whether the free gas was connected with the gas blowouts that occurred in the inner layer of the permafrost.

In this study, we reconstructed the permafrost structure of the Qilian Mountains using a combination of methods, and measured the permeability of methane in the ice-bearing sediment permafrost. A relationship between the ice saturation of the permafrost and methane permeability was established, which permitted the quantitative evaluation of the sealing ability of the permafrost with regards to methane migration. In addition, we collected published data of core headspace gases and hydrate-bound gases from gas hydrate wells in the Qilian Mountains in order to determine the source of the shallow gas. Based on this examination, we suggest a new gas hydrate petroleum system associated with the sealing ability of permafrost.

2. Geological setting

2.1 Geological background and gas hydrate reservoir

The Qilian Mountains are located in the northeastern part of the Qinghai–Tibetan Plateau in China, and have approximately 10^5 km^2 of permafrost cover,[19] and the mountains thus represent one of the plateau's most important Alpine permafrost sources.[20,21] The "Scientific Drilling Project of Gas Hydrate" is located in the Muri coalfield of the Qilian Mountains (Fig. 1), which is at an altitude of 4000–4300 m, has a mean annual ground temperature of −2.4 °C, and has widespread (but discontinuous) coverage of permafrost.[22] Permafrost thickness, measured and estimated from wireline logging, ranges from 60 to 95 m, although it can exceed 100 m in large parts of the region.[19,22,23]

The area discussed in this study is situated in the western part of the Middle Qilian tectonic block, which formed during the Caledonian Movement (513–386 Ma) and is adjacent to the South Qilian structural zone.[24,25] It is also situated in the Muri Depression of the South Qilian Basin.[26,27] The Juhugeng ore field is one of the major divisions of the Muri coalfield. The middle part of this ore field is characterized by Triassic strata that have been folded into an anticlinal structure, whereas the northern and southern parts are represented by two synclines composed of Jurassic lacustrine coal-bearing strata. Large thrust faults cut across the northern and southern flanks of the anticline and synclines. In the two synclines, thrust faulting has caused a series of additional northeast-trending shear fractures to develop, forming structural depressions in the displaced blocks. Therefore, the study area contains belts running from north to south and zones running from west to east (Fig. 1).[28,29]

Exposed strata in the Juhugeng ore field are mainly of Quaternary, Middle Jurassic, and Upper Triassic age. The Upper Triassic basement is widely exposed in the northern and southern regions. The lithologies defining the anticline axes mostly include black siltstone, mudstone, and thin coal seams, and these units form parallel nonconformities when in contact with the overlying Jurassic strata. The Middle Jurassic strata include the Muri and Jiangcang formations, both of which may be divided into upper and lower members based on their respective lithologies and interpretations of their depositional environments. The lower member of the Muri Formation formed in a braided river–alluvial plain environment, and is characterized by coarse clastic rocks that occasionally contain thin carbonaceous mudstones or coal seams, all of which overlie a basal conglomerate. The upper member formed in a lacustrine–marshy environment, and it is characterized by dark gray siltstone, fine-grained sandstone, gray fine- or medium-grained sandstone, and coarse-grained sandstone with two thick coal seams. By contrast, the lower member of the Jiangcang Formation formed in a deltaic–lacustrine environment, is characterized by gray fine- and medium-grained sandstone, dark gray mudstone and siltstone, and is located between two and six layers of coal. The upper member formed in shallow and deep lacustrine environments and is characterized by fine-grained clastic mudstone, siltstone, gray siltstone, black-brown oil shale, and lenticular siderite. Quaternary units are abundant in the drilling area, and include soil, alluvial sand, gravel, and angular gravel.[9]

The combined information from drilling and core experiments shows that gas hydrates occur mainly in the Jiangcang Formation of the Middle Jurassic in the Muri permafrost. Fracture filling is the main process by which gas hydrate occurs, forming as thin-layer-like flakes and block groups on the fracture surfaces of the siltstone, mudstone, and oil shale. Pore-filled hydrate occurs in the porous sandstone. It is difficult to

observe by the naked eye, but its presence can be speculated indirectly by the continuously emerging bubbles and water drops, and the dispersion-like abnormally low temperature of infrared imaging from the core.[9,17] In addition, the gas hydrates are distributed non-continuously in the vertical direction in each borehole, and the lateral distribution of hydrate between the boreholes is not apparent because the rock fracture system plays an important role in gas hydrate distribution.[17] Preliminary estimation indicates that there is a potentially rich source of the gas hydrate in this region.[30] The specific geological characteristics of the gas hydrate reservoir have been summarized by Wang *et al.*,[11] as shown in Table 1.

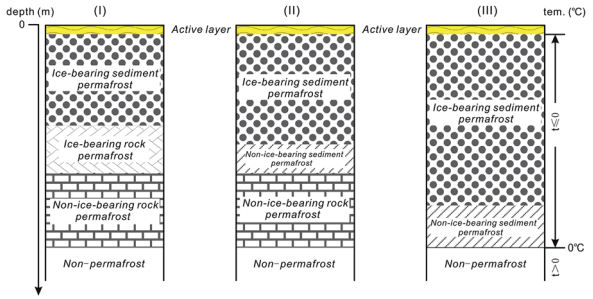

Fig. 3 Permafrost structure types found in the Qinghai–Tibetan Plateau, as confirmed by drilling.

2.2 Permafrost structure types

Several test drillings for gas hydrate have been implemented in the Qilian Mountains and Qiangtang Basin of the Qinghai–Tibetan Plateau by the China Geological Survey since 2008. The depths of the drillings have ranged from 173.84 to 882.01 m. The obtained core and well-temperature data help us understand better the structure of the permafrost in the Qinghai–Tibetan Plateau. In China, permafrost generally refers to a variety of soils and rocks bearing ice at or below 0 °C; ice-free soils/rocks at or below 0 °C are known as cold soils/rocks.[19] However, in North America, soils and rocks at or below 0 °C are called permafrost, irrespective of whether they contain ice. As permafrost in the Qinghai–Tibetan Plateau is composed of unconsolidated sediments and rocks, different sediment/rock types and degrees of ice saturation will cause differences in the formation pressure and sealing ability of the permafrost, thereby affecting gas hydrate reservoirs. In order to discuss the effect of the structure of permafrost on gas hydrate reservoirs, we summarized three types of permafrost structure according to the ice conditions and rock/sediment types on the Qinghai–Tibetan Plateau, based on core and well-temperature data (Fig. 3). Type I, composed of ice-bearing sediment permafrost, ice-bearing rock permafrost, and non-ice-bearing rock permafrost from top to bottom, is the main permafrost structure. Type II involves a thicker, porous and permeable sediment layer and is composed of ice-bearing sediment permafrost, non-ice-bearing sediment permafrost, and non-ice-bearing rock permafrost. Type III occurs when sediment thickness is greater than permafrost thickness, and comprises ice-bearing sediment permafrost and non-ice-bearing sediment permafrost. In addition, for Type I, when the thickness of the ice-bearing sediment permafrost is zero, the permafrost is composed of ice-bearing rock permafrost and non-ice-bearing rock permafrost only, which is unfavorable for gas hydrate accumulation because of its poor sealing ability.

During gas hydrate explorations in the Qilian Mountains, Type I permafrost structures were encountered widely. For 10 wells (DK-1 to DK-10), the only difference was in the thickness of the ice-bearing sediment permafrost. Drilling observations showed that the thickness of the active layer was about 1–2 m, where the fine clay was silt-like, and the coarse gravel was mixed and poorly sorted. In the layer of ice-bearing sediment permafrost, there were sediments cemented by ice, and in some cases vein-like, reticular, massive, layered, and fractured ice occurred within the sediments. In the layer of ice-bearing rock permafrost, ice mainly filled the fractures within the rock with small amounts of fine to coarse-grained sandstones.

3. Materials and methods

3.1 Methane permeability experiments

Type I permafrost structures were encountered widely in the Qilian Mountains. Without considering the sealing ability of the

Table 1 Geological characteristics of gas hydrate in the Qilian Mountains permafrost (modified after Wang *et al.*, 2014)

Properties	Value and characteristics	Source
Location	Juhugeng orefield	Zhu *et al.*[9]
Thickness of permafrost	60–95 m; 100 m (local)	Zhou *et al.*,[19] Zhu *et al.*,[22] Pan *et al.*[23]
Mean annual ground temperature	−2.6 °C	Zhu *et al.*[22]
Geothermal gradient	Within permafrost: 0.030 °C m^{-1}; below permafrost: 0.022 °C m^{-1}	Zhu *et al.*[22]
Depth of the hydrate pay zone	133–396 m	Zhu *et al.*,[9] Lu *et al.*[67]
Occurrence type	Fracture filling, pore filling	Zhu *et al.*,[9] Wang *et al.*[17]
Hydrate color	White, milky white, wheat	Zhu *et al.*[9]
Reservoir lithology	Mudstone, oil shale, siltstone, fine sandstone	Zhu *et al.*,[9] Wang *et al.*[17]
Reservoir formation	Jiangcang formation (J_2)	Zhu *et al.*[9]
Gas hydrate saturation	13–86%	Guo and Zhu[68]
Gas composition	54–76% CH_4, 8–15% C_2H_6, 4–21% C_3H_8, 17% CO_2	Zhu *et al.*[9]
Gas source	Thermo-genesis	Zhu *et al.*,[9] Lu *et al.*,[28,67] Huang *et al.*[31]
Pore water salinity	7.5–8.0‰	Wang *et al.*[18]
Associated mineral	Calcite, pyrite, alstonite, ankerite	Wang *et al.*[10,11,17,18]

rock with regards to methane migration, the degree of ice saturation of the sediment limits methane migration by changing the porosity. In order to obtain ideal data of methane permeability in ice-bearing sediment permafrost, seepage tests using synthesized specimens with uniform scattering of ice in the pores of the medium were conducted to establish the effect of the degree of ice saturation.

3.1.1 Sediment specimen preparation. The sediment samples used in the tests were fine silty sands with a specific gravity of 2.69, maximum void ratio of 0.95, and minimum void ratio of 0.45. The specimens, which had a porosity of 40% and dry density of 1.6 g cm^{-3}, were prepared with diameters and heights of 39.1 and 80 mm, respectively, in a copper mold.

3.1.2 Test apparatus. Tests were conducted in an apparatus developed at the Institute of Mechanics, Chinese Academy of Sciences (Fig. 4). The apparatus provided confining pressures by hydraulic loading ranging from 0–30 MPa with an accuracy of 0.5%, and the pressure was imposed with reference to the practical formation pressure. A cold room was used to maintain the test temperature between −20 and +20 °C with an accuracy of 2.5%. An inlet was set to provide gas flow into the specimen *via* a gas cylinder with a maximum pressure of 10 MPa. The backpressure provided by a fluid-filled pump ranged from 0–10 MPa. Transducers were used to monitor the pressure and temperature during the tests. The samples were wrapped in a butyl rubber membrane to keep them separated from the load fluid. This setup allowed low-temperature conditions for the formation of ice-bearing sediments and permeability measurements in an integrated system.

The gas flow rate was calculated by both a gas flow meter and a gas collection system. The gas flow meter, which had a capacity of 500 mL min^{-1} and accuracy of 0.1%, was used to measure the instantaneous gas flow rate percolating into the specimen. The gas collection system had a volume of 6 L, and it was designed to measure the gas flow rate exiting the specimen (Fig. 5). In this system, the water in two cylinders was pushed out by the methane gas flowing out of the specimen. The gas volume was equal to that of the displaced water, which was measured by an electronic balance with a range of 0 to 600 g and accuracy of 0.01 g. This is possible because the gas volume under a pressure of 0.1 MPa and temperature of 273.15 K is almost equal to that of the displaced water (the solubility of methane in water under these conditions is negligible). When the gas flow in the specimen was stable, the two calculated methods agreed.

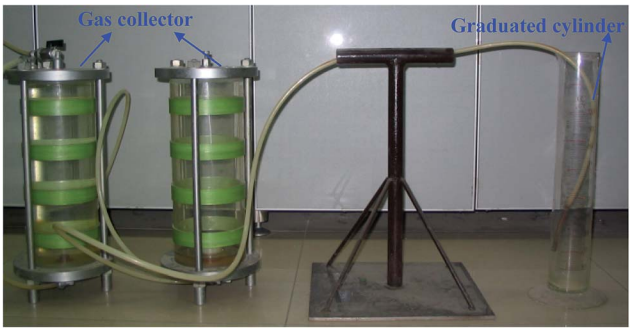

Fig. 5 Gas collection system.

3.1.3 Test procedure. The procedure of the formation of ice-bearing sediments and seepage tests was as follows:

(1) Each specimen with an initial porosity of 40% (specific gravity: 2.65, dry density: 1.6 g cm^{-3}) was sealed within a butyl rubber membrane, placed into the triaxial cell, evacuated, and water absorbed into the pores until a desired water content was reached (water volumes V_W injected are listed in Table 2). The specimens were frozen at a temperature of −10 °C in the cold room for two days, at which time the ice-bearing sediments were formed. Here, the effect of unfrozen water was not considered and, therefore, the degree of ice saturation could be calculated based on the assumption of the complete transformation of the absorbed water to ice, *i.e.*, by the equation: $S_i = \frac{\alpha V_w}{V_p}$ (where S_i, α, V_w, and V_p indicate the ice saturation, volume swelling coefficient from water to ice (1.1), volume of injected water, and volume of pore spaces, respectively).

(2) After specimen formation, a 5 MPa confining pressure was applied to simulate the formation pressure under permafrost conditions and to avoid the escape of methane gas through the voids of the membrane and specimen. Then, methane gas at a temperature of −2 °C (pre-chilled in the cold room) was forced into the specimen under pressure. The pressure differences were controlled by a pressure regulator valve until the displaced water flow became constant. Finally, the water flow rate and pressure difference were recorded, as displayed in Fig. 6.

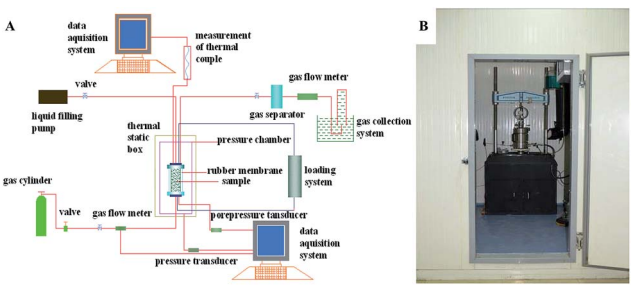

Fig. 4 Apparatus used for (A) ice-bearing sediment syntheses and (B) triaxial tests.

Table 2 Water volume *versus* ice saturation in sediments

Water volume (mL)	Ice saturation
0	0
13	0.36
16	0.47
16	0.47
21	0.6
21	0.6
24	0.7
28	0.8
30	0.88
31	0.9

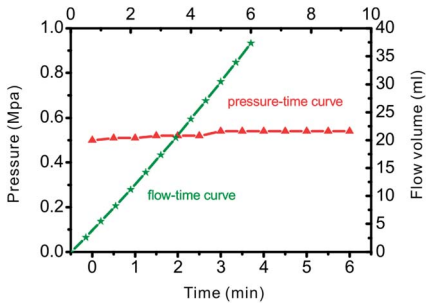

Fig. 6 Gas flow volume and pressure with time.

The permeability was calculated by Darcy's law as follows: $K = \frac{Q\mu L}{A\Delta P}$ (where K, Q, μ, ΔP, L, and A indicate the absolute gas permeability, gas flow rate, gas viscosity, gas pressure difference, and length and sectional area of the specimen, respectively).

3.2 Gas data for gas source analysis

Several researchers have previously conducted isotopic, compositional, and structural analyses of hydrate and core headspace gas samples from drilling wells in the Qilian Mountains permafrost.[9,10,28–32] They have indicated that these gases are thermogenic in origin with minor additions of mixed microbial and thermogenic methane. As gas blowouts mainly occurred in the shallow formations, their genesis should relate directly to shallow gas characterization. However, there were no detailed descriptions for shallow gas genetic characterization and the relationship between shallow and hydrate-bound gases in those previous studies. Data of hydrate-bound and core headspace gases, collected from three gas hydrate wells, have been collected in this study (Table 3) in order to re-analyze the sources of the gases and to discuss their relationships.

4. Results and discussion

4.1 Relationship between ice saturation and methane permeability

The results of the methane permeability tests (Table 4) show that the permeability of ice-bearing sediments decreases as ice saturation increases, and points of inflection occur at different ice saturation intervals. When ice saturation reaches 60%, permeability reduces to 1/100. When ice saturation reaches 80%, permeability reduces to 10^{-6}, which is representative of an ultra-low-permeability porous media (Fig. 7).

Table 4 Methane permeability changes with ice saturation

Experiment no.	Ice saturation	Permeability (Darcy)
1	0	2.7000
2	0.09	1.5000
3	0.17	0.9430
4	0.36	0.5350
5	0.47	0.4000
6	0.48	0.3980
7	0.59	0.0259
8	0.61	0.0267
9	0.71	0.0255
10	0.72	0.0259
11	0.81	0.0000213
12	0.88	0
13	0.91	0

The mechanism of seepage in ice-bearing sediment is illustrated in Fig. 8. The pore structure of the ice-bearing sediment is regarded as having ideal pore spaces and pore throats, in which the pore spaces are larger than the connected pore throats. Therefore, the pore spaces play an important role in fluid capture and storage and the pore throats control the flow of the fluid (Fig. 8A). When ice forms in the pores, it first occupies the pore spaces because of the relatively small capillary pressure; therefore, the percolation paths are narrowed and gas permeability is partially reduced (Fig. 8B). With the increase of ice saturation, ice occupies most of the pore spaces and penetrates into the pore throats, which means that the percolation paths become increasingly blocked and gas permeability is reduced further, even becoming impermeable (Fig. 8C).

4.2 Origin of shallow gas derived from isotopic and compositional analyses

The stable carbon isotope signature of methane from gas hydrates is commonly used to determine whether the methane was microbially or thermally produced. Pure microbial methane typically has $\delta^{13}C$ values in the range of $-90‰$ to $-60‰$, while pure thermogenic methane has $\delta^{13}C$ values in the range of

Table 3 Depths of hydrate-bound gases and core headspace gases collected from gas hydrate wells in the Qilian Mountains permafrost

Well no.	Depth of hydrate pay zone (m)	Gas sample type	Depth of gas samples (m)	Gas data source
DK-1	133.5–170.5	Hydrate-bound gas	>133.5	Lu *et al.*[67]
DK-2	144.4–387.5	Core headspace gas	55.3–450.7	Huang *et al.*[31]
DK-8	148.20–304.28	Core headspace gas	104–398	Lu *et al.*[32]

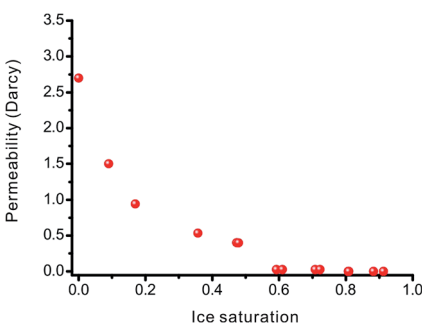

Fig. 7 Methane permeability changes with ice saturation.

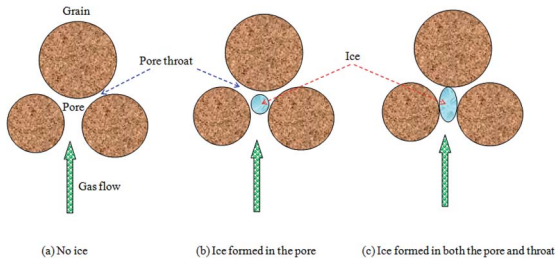

Fig. 8 Mechanism of seepage in ice-bearing sediment.

−50‰ to −20‰.[33,34] Gases containing mixtures of microbial and thermogenic methane, however, are characterized by a broad range of values determined by the relative contributions and $\delta^{13}C$ values of the microbial and thermogenic end members.[35] The relationship of the methane carbon isotope composition *versus* the ethane and propane molecular composition of the hydrate-bound and core headspace gases, collected from gas hydrate wells in the Qilian Mountains, shows that (1) hydrate-bound and core headspace gases collected from the hydrate pay zone are mainly thermogenic in origin, with minor additional mixed microbial and thermogenic methane; (2) core headspace gases collected from the layers above the hydrate pay zone are shallow gases, which are mainly of mixed origin, *i.e.*, mixed thermogenic and microbial methane, with minor thermogenic; (3) the value of the methane carbon isotope composition of the shallow gases is less than and has a narrower range of variation than gases from the hydrate pay zone; (4) the volumetric hydrocarbon gas ratio (R) of $C_1/(C_2 + C_3)$ of the shallow gases is greater than and has a wider range of variation than gases from the hydrate pay zone (Fig. 9). The similar methane carbon isotope composition of the shallow gases indicates that the gases came from the same source. The greater and wider-ranging R-values of the shallow gases show obvious fractionation in the chemical composition during migration and preferential migration of methane molecules compared with heavy hydrocarbon molecules.

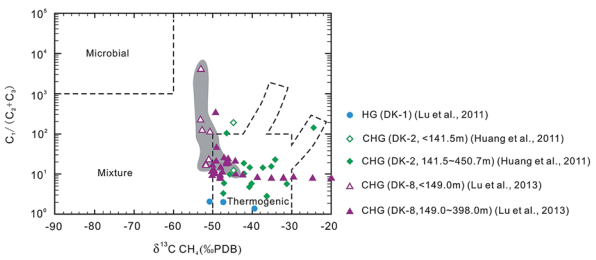

Fig. 9 Relationship between methane carbon isotope composition and ethane and propane molecular compositions of the hydrate-bound gases (HG) and core headspace gases (CHG) collected from gas hydrate wells in the Qilian Mountains. Solid symbols indicate samples from the hydrate pay zone, hollow symbols indicate samples from the layers above the hydrate pay zone, gray area indicates shallow gas primarily originating from thermogenic sources (diagram modified after Bernard *et al.*[33]).

As the gas hydrate system in the Qilian Mountains permafrost is considered an epigenetic hydrocarbon reservoir situated over a deep-seated hydrocarbon reservoir,[10] the low-temperature hydrate reservoir, controlled by P–T conditions, would not only capture the deeper hydrocarbon gas that migrated upward along the fault system, but also prevent gas escaping from the GHSZ. Clearly, the contribution of deeper gas to the shallow gas is very limited. Meanwhile, the value of $\delta^{13}C_{PDB}$ of methane from the shallow gas is greater than −54%, indicating that the contribution of microbial gas to the shallow gas is also limited. Consequently, the gas hydrate reservoir has become a major supplier of hydrocarbon gas to the shallow gas because of its metastability. Wang *et al.*[11] suggested that the GHSZ in the Qilian Mountains has migrated and shrunk, and they additionally inferred that the permafrost degeneration resulting from climatic warming is the most direct cause for GHSZ migration. It is difficult to speculate, but it is possible that when the top of GHSZ moved downward, gas hydrates occurring at the top of the GHSZ decomposed and released methane gas, which migrated upward into the shallow formation along the fault system. Low-temperature hydrate has a strong sealing ability, which has been confirmed by measurements of trace element concentrations; these measurements can be interpreted to demarcate the base of the gas hydrate layer in the Qilian Mountains.[10] Similarly, the gas hydrate layer can also reduce the activity of the gas molecules. The sealing ability of hydrate layer and lower porosity and lower permeability of the reservoir can greatly limit the upward migration of gas. When the bottom of the GHSZ moved upward, the gas hydrates that occurred at the bottom of the GHSZ decomposed and released methane gas, which migrated upward into the new GHSZ along the fault system and then re-formed as gas hydrates. Thus, gas decomposed from gas hydrates at the top of the original GHSZ was the main source of the shallow gas. The uniform gas source resulted in the similar methane carbon isotope composition of the shallow gas. The decomposition process of gas hydrates drove the methane molecules to migrate preferentially and ultimately led to the greater and wider-ranging R-values of the shallow gas.

4.3 Shallow gas pool formation and gas hydrate petroleum system

Gas hydrates are proposed to have exerted a major control on past climates, both for the glacial–interglacial periods,[36,37] and also for other important geological events extending back to the start of the Phanerozoic or earlier.[38,39] The gas hydrate formation in the Qilian Mountains permafrost was closely related to the uplift of the Qinghai–Tibetan Plateau that caused the permafrost formation. Since the Pleistocene, this plateau has undergone several successive uplifts until the late Pleistocene (11–25 kaBP), when elevations reached 4000 to 4500 m. Due to the high altitude, the plateau has temperature conditions conducive to permafrost formation and preservation. Ever since the Glacial Maximum was reached in the Late Pleistocene, the main body of the permafrost has formed in the plateau.[19] Some infer that episodic atmospheric methane flux, attributed to massive gas hydrate destabilization, commonly called the

"clathrate gun" hypothesis,[37] is the trigger for, or a significant cause of, important global climate changes including glacial–interglacial transitions.[40]

Global climate warming is an indisputable fact. According to the Fourth Assessment Report of the IPCC,[41] the global surface temperature will increase by 1.1–6.4 °C by the end of the 21st century. Empirical evidence has indicated strongly that effects related to climatic warming are well underway in the polar regions[42–48] and Qinghai–Tibetan Plateau.[20,21,49–61] Climatic warming can lead to an increase in permafrost temperature, thickening of the active layer, and reduction in the percentage of the terrestrial surface underlain by near-surface permafrost.[42,62–64] For example, in the Qinghai–Tibetan Plateau, the trend is for the active layers of permafrost regions to become thicker under the impact of global warming.[57] Numerical simulations by Yang *et al.*[59,60] have indicated that air temperature on the Qinghai–Tibetan Plateau will continue to increase during the 21st century and significant warming has already resulted in extensive degradation of the permafrost. Gradual climatic warming has also affected the stability of the gas hydrate below the permafrost and caused the migration and reduction of the GHSZ,[65] evidence for which has been found in the Qilian Mountains from minerals related to gas hydrates. A study on the morphology and sulfur isotopes of fracture-filling pyrites from two gas hydrate drilling sites in the Qilian Mountains confirmed that the top and the bottom of GHSZ have moved downward and upward by up to 51.5–71.43 m and 52.5–69.7 m, respectively. By inference, the thickness of permafrost has decreased by about 10–13 m.[11]

Isotopic and chemical compositional analyses of the shallow gas in the Qilian Mountains permafrost shows that methane gas decomposed from gas hydrates at the top of the original GHSZ was the main source of the shallow gas, as described in Section 4.2. Based on the relationship between ice saturation and methane permeability in ice-bearing sediments, we established that ice-bearing sediments with different degrees of ice saturation have different sealing abilities with regards to methane migration. When ice saturation is >80%, methane gas can be completely sealed within the permafrost. In the actual geological environment, 10 cm-thick layers of ice were often drilled in the Qilian Mountains. Thus, the layer of permafrost in the Qilian Mountains generally has a high ice-saturation property. When methane gas decomposed from gas hydrates migrated upward along the fault system and encountered an ice-bearing permafrost with high ice saturation (S_i > 80%), one kind of shallow gas pool began to form under the layer of permafrost (Fig. 10). Gas blowouts also indicated the existence of the shallow gas pool. By this token, the formation of the shallow gas pool is related to a metastable gas hydrate reservoir controlled by the *P*–*T* conditions, sealing ability of permafrost, and fault system. Climatic warming was the main driving force behind the formation of the shallow gas pool. The volume of the gas pool was controlled by the amount of hydrate decomposition that resulted from the GHSZ reduction, gas transmission capacity of the fault system, and gas storage capacity of reservoir rocks/sediments.

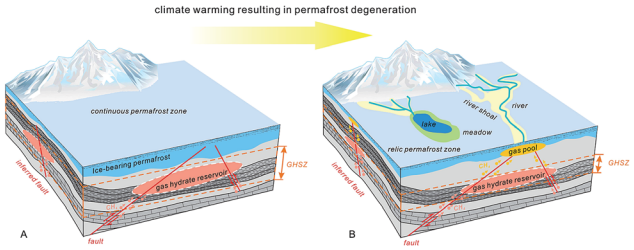

Fig. 10 Evolution of gas hydrate petroleum system in the Qilian Mountains permafrost: (A) end of Late Pleistocene and (B) modern day. GHSZ indicates gas hydrate stability zone.

The gas hydrate petroleum system in the Qilian Mountains is dynamic because of the permafrost degeneration (Fig. 10). It is generally believed that thermal conditions conducive to the formation of permafrost and gas hydrate have persisted in the Qinghai–Tibetan Plateau since the end of Late Pleistocene,[19] when the gas hydrate petroleum system in the Qilian Mountains was an epigenetic hydrocarbon situated over a deep-seated hydrocarbon reservoir (Fig. 10A). As climatic warming resulted in permafrost degeneration, the gas hydrate reservoir was reduced and the shallow gas pool formed under ice-bearing permafrost with high ice saturation (Fig. 10B). Currently, the gas hydrate petroleum system in the Qilian Mountains is composed of a deep-seated hydrocarbon reservoir, gas hydrate reservoir, and shallow gas pool, which are connected *via* the fault system. Clearly, the relationship between climatic change and the gas hydrate petroleum system in the Qilian Mountains is very close.

In gas hydrate petroleum systems, the formation of a shallow gas pool is indicative that climatic warming is already causing permafrost degradation and the reduction of the gas hydrate reservoir. It is easy to hypothesize that with further permafrost thinning and the degree of ice saturation falling below 80% in the ice-bearing permafrost, methane gas will no longer be sealed. From an energy perspective, the increasing volume of the gas pool means that it will likely become a shallow gas resource available for exploitation; however, for the environment, the gas pool is an underground "time bomb" that is a potential source of greenhouse gas.

5. Conclusions

(1) The test results of methane permeability show that the permeability of ice-bearing sediments decreases as ice saturation increases; when ice saturation is >80%, methane gas can be completely sealed within the permafrost.

(2) The value of the methane carbon isotope composition of the shallow gas is less than and has a narrower range of variation than the gas from the hydrate pay zone. The *R*-value of the shallow gas is greater than and has a wider range of variation than the gas from the hydrate pay zone. Methane gas decomposed from gas hydrates at the top of the original GHSZ was the main source of the shallow gas.

(3) A shallow gas pool has developed in the gas hydrate petroleum system within the Qilian Mountains permafrost. Its formation was related to a metastable gas hydrate reservoir controlled by the *P–T* conditions, sealing ability of the permafrost, and fault system. Climatic warming was the main driving force behind the formation of the shallow gas pool. The volume of the gas pool was controlled by the amount of hydrate decomposition that resulted from the GHSZ reduction, gas transmission capacity of the fault system, and gas storage capacity of reservoir rocks/sediments.

(4) The gas hydrate petroleum system within the Qilian Mountains permafrost has been dynamic since the end of the Late Pleistocene because of permafrost degeneration. Currently, the gas hydrate petroleum system is composed of a deep-seated hydrocarbon reservoir, gas hydrate reservoir, and shallow gas pool, which are connected *via* the system. The relationship between climate change and the gas hydrate petroleum system is very close.

Acknowledgements

We thank the anonymous reviewers and publishing editor (Dr Jack Busby from Royal Society of Chemistry) for their many useful comments and suggestions, which helped improve the paper. This work was funded by the National Natural Science Foundation of China (Grant no.: 41102021, 41202099), National Special Research Fund (Gas Hydrate Resource Exploration and Production Testing Project) (Grant no.: GZHL20110308, GZH201400301), and Chinese Polar Environment Comprehensive Investigation & Assessment Programmes (Grant no.: CHINARE2014-04-05).

References

1 E. Sloan and C. Koh, in *Clathrate Hydrates of Natural Gases*, CRC Press, 3rd edn., 2008.
2 R. Boswell and T. S. Collett, *Energy Environ. Sci.*, 2011, **4**, 1206–1215.
3 Y. F. Makogon, S. A. Holditch and T. Y. Makogon, *J. Pet. Sci. Eng.*, 2007, **56**, 14–31.
4 K. A. Kvenvolden and T. D. Lorenson, *Am. Geophys. Union*, 2001, **124**, 3–18.
5 T. Zhang, R. G. Barry, K. Knowles, J. A. Heginbottom and J. Brown, *Polar Geography*, 1999, **23**(2), 147–169.
6 T. S. Collett, M. W. Lee, W. F. Agena, J. J. Miller, K. A. Lewis, M. V. Zyrianova, R. Boswell and T. L. Inks, *Mar. Pet. Geol.*, 2011, **28**(2), 279–294.
7 S. R. Dallimore and T. S. Collett, *Geology*, 1995, **23**(N6), 527–530.
8 S. R. Dallimore and T. S. Collett, *Geol. Surv. Can. Bull.*, 2005, **585**, 140.
9 Y. Zhu, Y. Zhang, H. Wen, Z. Lu, Z. Jia, Y. Li, Q. Li, C. Liu, P. Wang and X. Guo, *Acta Geol. Sin. (Engl. Ed.)*, 2010, **84**(1), 1–10.
10 P. Wang, X. Huang, S. Pang, Y. Zhu, Z. Lu, S. Zhang, H. Liu, K. Yang and B. Li, *Mar. Pet. Geol.*, 2015, **59**, 72–90.
11 P. Wang, Y. Zhu, Z. Lu, X. Huang, S. Pang and S. Zhang, *Cold Reg. Sci. Technol.*, 2014, **98**, 8–17.
12 R. Boswell, G. Moridis, M. Reagan and T. S. Collett, *Seventh International Conference on Gas Hydrate*, Edinburgh, Scotland, 2011.
13 C. A. Koh, A. K. Sum and E. D. Sloan, *J. Nat. Gas Sci. Eng.*, 2012, **8**, 132–138.
14 T. S. Collett, Proceedings of the 1st International Conference on Natural Gas Hydrates, *Ann. N. Y. Acad. Sci.*, 1993, **715**, 247–269.
15 V. S. Yakushev and E. M. Chuvilin, *Cold Reg. Sci. Technol.*, 2000, **31**, 189–197.
16 2013 Annual Report. Oil and Gas Survey of China Geological Survey, 2014 (in Chinese).
17 P. Wang, Y. Zhu, Z. Lu, X. Guo and X. Huang, *Geol. Bull. China*, 2011, **30**(12), 1839–1850.
18 P. Wang, Y. Zhu, Z. Lu, X. Huang, S. Pang, S. Zhang and K. Yang, *Miner. Deposita*, 2013, **32**(5), 1045–1056.
19 Y. Zhou, D. Guo, G. Qiu and S. Li, *China Permafrost*, Science Press, Beijing, 2000 (in Chinese).
20 J. Wu, Y. Sheng, H. Yu and J. Li, *J. Glaciol. Geocryol.*, 2007, **29**(3), 418–425.
21 Q. Wu, X. Dong, Y. Liu and H. Jin, *Arct. Antarct. Alp. Res.*, 2007, **39**(4), 682–687.
22 Y. Zhu, Y. Liu and Y. Zhang, *Geol. Bull. China*, 2006, **25**(1–2), 58–63.
23 Y. Pan, G. Tian, A. Luan, N. Xu and P. Zhang, *Coal Geol*, China, 2008, 20(12), pp. 7–9.
24 Y. Feng, *Adv. Earth Sci.*, 1997, **12**(4), 307–314.
25 X. Zhang and S. Yang, *Study on Plate Tectonics in Qinghai Province: A Handbook for 1:1,000,000 Geo-Tectonic Map in Qinghai Province*, Geological Publishing House, Devon, U.K., 2007, pp. 1–221.
26 J. Fu and L. Zhou, *Northwest Geosci.*, 1998, **19**(2), 47–54.
27 J. Fu and L. Zhou, *Northwest Geosci.*, 2000, **21**(2), 64–72.
28 Z. Lu, Y. Zhu, Y. Zhang, H. Wen, Y. Li, Z. Jia, P. Wang and Q. Li, *Geosci.*, 2011, **24**(3), 581–588.
29 Z. Lu, Y. Zhu, H. Liu, Y. Zhang, C. Jin, X. Huang and P. Wang, *Mar. Pet. Geol.*, 2013, **43**, 341–348.
30 Z. Lu, Y. Zhu, Y. Zhang, H. Wen, Y. Li and P. Wang, *Geol. Bull. China*, 2010, **29**(9), 1310–1318.
31 X. Huang, Y. Zhu, P. Wang and X. Guo, *Geol. Bull. China*, 2011, **30**(12), 1851–1856.
32 Z. Lu, Z. Rao, Y. Zhu, H. Liu and Y. Zhang, *Acta Geol. Sin*, 2013, **87**(8), 1167–1178.
33 B. B. Bernard, J. M. Brooks and W. M. Sackett, *J. Geophys. Res-Oc. Atm.*, 1978, **83**(NC8), 4053–4061.
34 M. J. Whiticar, *Chem. Geol.*, 1999, **161**, 291–314.
35 J. W. Pohlman, E. A. Canuel, N. R. Chapman, G. D. Spence, M. J. Whiticar and R. B. Coffin, *Org. Geochem.*, 2005, **36**, 703–716.
36 E. G. Nisbet, *Philos. Trans. R. Soc., A*, 2002, **360**, 581–607.
37 J. P. Kennett, K. G. Cannariato, I. L. Hendy and R. J. Behl, *Methane Hydrates in Quaternary Climate Change: the Clathrate Gun Hypothesis*, American Geophysical Union, Washington, D.C., 2003, p. 216.

38 M. J. Benton and R. J. Twitchett, *Trends Ecol. Evol.*, 2003, **18**, 358–365.
39 J. L. Kirschvink and T. D. Raub, *C. R. Geosci.*, 2003, **335**, 65–78.
40 J. Majorowicz, J. Safanda and K. Osadetz, *Clim. Past*, 2012, **8**, 667–682.
41 IPCCClimate Change 2007: The Physical Science Basis, *Contribution of Working Group I to the Fourth Assessment Report of the Intergovernmental Panel on Climate Change*, Cambridge University Press, Cambridge, U.K, 2007.
42 O. Anisimov and S. Reneva, *Ambio*, 2006, **35**(4), 169–175.
43 J. Hansen, M. Sato, J. Glascoe and R. Ruedy, *Proc. Natl. Acad. Sci. U. S. A.*, 1998, **95**(8), 4113–4120.
44 J. Morison, K. Aagaard and M. Steele, *Arctic*, 2000, **53**(4), 359–371.
45 T. E. Osterkamp, *Global. Planet. Change*, 2005, **49**, 187–202.
46 M. C. Serreze, J. E. Walsh, F. S. Chapin, III, T. Osterkamp, M. Dyurgerov, V. Romanovsky, W. C. Oechel, J. Morison, T. Zhang and R. G. Barry, *Clim. Change*, 2000, **46**(1–2), 159–207.
47 J. Smith, R. Stone and J. Fahrenkamp-Uppenbrink, *Science*, 2002, **297**(5586), 1489.
48 K. M. Walter, S. A. Zimov, J. P. Chanton, D. Verbyla and F. S. Chapin, III, *Nature*, 2006, **443**, 71–75.
49 G. Cheng and T. Wu, *J. Geophys. Res.*, 2007, **112**, FO2S03.
50 X. Li and G. Cheng, *Sci. China, Ser. D: Earth Sci.*, 1999, **42**(1), 72–79.
51 Z. Nan, Z. Gao, S. Li and T. Wu, *Acta Geograph. Sin.*, 2003, **58**(6), 817–823.
52 C. Tong and Q. Wu, *Cold Reg. Sci. Technol.*, 1996, **24**, 101–106.
53 S. Wang, *Arid Land Geol.*, 1993, **16**(1), 1–18.
54 S. Wang, H. Jin, S. Li and L. Zhao, *Permafr. Periglac. Process.*, 2000, **11**, 43–53.
55 Q. Wang, L. Lin, D. Li, *et al.*, *Plateau Meteorology*, 2005, **24**(5), 708–713.
56 Q. Wu and Y. Liu, *Cold Reg. Sci. Technol.*, 2004, **38**, 85–92.
57 Q. Wu, Z. Lu and Y. Liu, *Adv. Clim. Change Res.*, 2006, **2**(suppl. 1), 77–80.
58 Q. Wu, G. Jiang, Y. Pu and Y. S. Deng, *Geol. Bull. China*, 2006, **25**(1–2), 29–33.
59 M. Yang, F. E. Nelson, N. I. Shiklomanov, D. Guo and G. Wan, *Earth Sci. Rev.*, 2000, **103**(1–2), 31–44.
60 Z. Yang, Y. Ou, X. Xu, L. Zhao, M. Song and C. Zhou, *Acta Ecol. Sin.*, 2010, **30**, 33–39.
61 L. Zhao, L. Chen, D. Yang, G. Cheng, Y. Ding and S. Liu, *Global. Planet. Change*, 2004, **43**, 19–31.
62 H. J. Akerman and M. Johansson, *Permafr. Peiglac. Process.*, 2008, **19**, 279–292.
63 S. A. Harris, *Effects of climatic change on northern permafrost Northern Perspectives*, The Canadian Arctic Resources, 1987, pp. 0380–5522, vol. 15, number 5.
64 W. Tucker, L. Brigham and F. Nelson, *J. Cold Reg. Eng.*, 2004, **18**(4), 123–133.
65 D. Chen, M. Wang and B. Xia, *Chin. J. Geophys.*, 2005, **48**(1), 165–172.
66 W. B. F. Ryan, S. M. Carbotte, J. O. Coplan, S. O'Hara, A. Melkonian, R. Arko, R. A. Weissel, V. Ferrini, A. Goodwillie, F. Nitsche, J. Bonczkowski and R. Zemsky, *Geochem., Geophys., Geosyst.*, 2009, **10**(3), Q03014.
67 Z. Lu, Y. Zhu, Y. Zhang, H. Wen, Y. Li and C. Liu, *Cold Reg. Sci. Technol.*, 2011, **66**, 93–104.
68 X. Guo and Y. Zhu, *Geol. Bull. China*, 2011, **30**(12), 1868–1873.